Rayleigh analysis of dielectric properties in textured $K_{0.5}Na_{0.5}NbO_3$ ceramics

Astri Bjørnetun Haugen,[1] Maxim I. Morozov,[1a)] Jacob L. Jones,[2] and Mari-Ann Einarsrud[1]

[1] Department of Materials Science and Engineering, Norwegian University of Science and Technology, Trondheim, Norway

[2] Department of Materials Science and Engineering, North Carolina State University, Raleigh, NC, USA

Abstract

Grain texturing is a known method of exploiting the intrinsic dielectric and piezoelectric anisotropy in ferroelectric ceramics. However, the role of crystallographic texture on anisotropic extrinsic contributions including domain wall motion is not yet understood. Here, we investigate the dielectric and piezoelectric properties and small signal dielectric nonlinearities in $K_{0.5}Na_{0.5}NbO_3$ ceramics in different directions of textured specimens and compare to ceramics without crystallographic texture. We demonstrate that directions in which pseudo-cubic <100> poles have greatest orientation density exhibit both an enhanced longitudinal piezoelectric response and lower dielectric nonlinearity.

1 Introduction

Dielectric nonlinearity is one of the key factors controlling precision and accuracy of functional devices based on ferroelectrics.[1-3] In conventional perovskite ferroelectrics, the dielectric

[a)] Corresponding author, electronic mail: maximm@alumni.ntnu.no

and piezoelectric response can be dominated by the motion of domain walls, even under subswitching conditions.[4-6] The motion of domain walls may include reversible[7] and irreversible[8] components, depending on the nature of their interaction with pinning centers such as point defects.[3] The irreversible motion of domain walls results in polarization hysteresis and nonlinearity that can be generally related using the Preisach formalism.[9] For the case of random distribution of pinning centers, the relationship between the dielectric nonlinearity and polarization hysteresis can be more simply described by the Rayleigh model, given by[2,10,11]

$$P(E) = \left(\varepsilon_r'(0) + \alpha E_0\right) E \pm \frac{1}{2}\alpha\left(E_0^2 - E^2\right) \tag{1}$$

$$\varepsilon_r' = \varepsilon_r'(0) + \alpha E_0 \tag{2}$$

where ε_r' is the real part of the relative dielectric permittivity, $\varepsilon_r'(0)$ is this permittivity extrapolated to zero electric field (E-field) amplitude, α is the Rayleigh constant, and E_0 is the E-field amplitude. The physical concept of the model correlates the irreversibility of domain wall displacement with the nonlinearity of the polarization response through the Rayleigh coefficient α. The value of α is a measure of the extent of irreversible domain wall displacement under an applied ac field, while $\varepsilon_r'(0)$ accounts for all linear dielectric contributions, including the intrinsic anisotropic response. The model has been justified for a large class of ferroics, albeit with exceptions.[12] In particular, it was found to adequately describe both lead-containing and lead-free piezoelectric ceramics,[11] including those based on $K_{0.5}Na_{0.5}NbO_3$ (KNN) .[13-15]

While the Rayleigh analysis of polarization response has been reported for numerous ceramics containing initially randomly oriented grains, anisotropic nonlinearity in crystallographically textured[16] ceramics can also be strongly influenced by anisotropic domain wall displacement. The use of crystallographic texture to enhance properties of ferroelectric materials has been historically motivated by a functional enhancement arising from the anisotropic intrinsic response.[16] However, we recognize here that texture can also influence the extrinsic contributions

due to factors such as grain-grain strain coupling, grain boundary pinning sites and electrical/dielectric percolation phenomena.[4,17]

The influence of grain texture on dielectric nonlinearity can be manifold. The alignment of strain from closely oriented grains has been shown to facilitate domain reorientation under fields of high amplitude in a bismuth titanate composition.[18] Our recent experiments in KNN[19] also demonstrated higher extents of domain switching under high electric field amplitudes in textured ceramics compared to those that were randomly oriented. If this phenomenon is also present at subswitching conditions, different nonlinearities in property coefficients due to domain wall motion may be expected in different directions of textured ferroelectric materials. Directions in which the polarization axes are strongly aligned through the initial grain texture and poling process may be expected to exhibit less nonlinear domain wall motion contributions when fields are applied parallel or closely parallel to that direction.

In this work we assess the anisotropic dielectric nonlinearity in textured KNN ceramics under subswitching electric field amplitudes. We then relate the different types of responses to the preferred orientation of the polar axes in the various configurations and likelihood of domain wall motion due to grain texturing and poling.

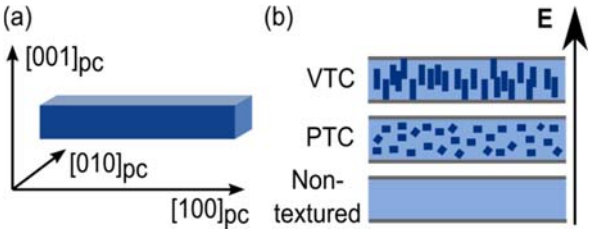

Figure 1. (a) Geometry and crystallographic directions (pseudocubic, pc) in the needle-like KNN templates used for texturing. (b) Orientation of the templates and subsequent direction of templated grain growth relative to the direction of the electric field for the three KNN samples investigated.

2 Experimental

KNN with $<100>_{pc}$ texture was synthesized by tape casting using needle-like KNN templates, followed by homotemplated grain growth during sintering at 1130 °C for 14 h in flowing O_2. A detailed description of the synthesis and the resulting microstructures are presented elsewhere.[19] Non-textured KNN was obtained by sintering uniaxially pressed submicron powders under the same conditions. Figure 1 (a) shows the geometry and crystallographic directions of needle-like KNN templates used for texturing. The configuration of the templates in the two textured ceramics, along with the non-textured KNN, are shown in Figure 1 (b). Planar template configuration (PTC) refers to a textured KNN where the tape cast direction (parallel to which the needle-like templates were aligned) is in the horizontal plane and parallel to the electrodes, and hence perpendicular to the applied E-field. Vertical template configuration (VTC) refers to a sample cut from the same piece of ceramic where the direction of template alignment is perpendicular to the electroded faces and thus parallel to the E-field. Table I reports selected characteristics of the respective specimens. The strong $<100>_{pc}$ preferred orientation parallel to the direction of the E-field in the VTC sample results in increased piezoelectric response compared to the non-textured KNN, while the PTC sample with a low degree of $<100>_{pc}$ preferred orientation has a lower piezoelectric response than the non-textured KNN (Table I).[19] In addition, the largest extent of non-180° domain reorientation as observed by prior *in situ* X-ray diffraction occurs in the VTC sample and is an order of magnitude higher than that observed in the PTC and non-textured KNN.[19]

Table I. Relative density (ρ), texture (Lotgering factor, F), piezoelectric constant (d_{33}) and normalized strain (S_{max}/E_{max}) for the samples used in this study. Data from ref. [19].

Sample	ρ (%)	F (%)	d_{33} (pC/N)	S_{max}/E_{max} (pm/V)
VTC	94	86	125±3	321±1
PTC	94	28	89±3	131±1
Non-textured	94	-	107±4	199±1

Dielectric permittivity was measured as a function of the E-field amplitude in the range 0.0028-2.8 kV/cm at frequencies of 1, 10, 100, 1 000 and 10 000 Hz with a Novocontrol Alpha A impedance analyzer (Hundsangen, Germany). The first measurements were performed on samples that had been aged for 1 year after application of strong poling electric fields (subsequently identified as "poled and aged"), before the samples were poled again at room temperature for 1-5 min at 20 kV/cm and measured after 24 h ("poled"). Next, the samples were poled for 60 min at 20 kV/cm while the temperature decreased from 200 to ~50 °C and measured after 24 h ("HT-poled"). Finally, the samples were thermally depoled at 475 °C for 60 min ("depoled"). The dielectric permittivity measurements were repeated after each step of poling, depoling, or aging. Linear regression was applied to the data measured at 100 Hz in order to extract the Rayleigh coefficient (α) and the initial dielectric permittivity ($\varepsilon_r'(0)$) within the Rayleigh regime.

3 Results and discussion

3.1 Rayleigh fit

All samples exhibited a Rayleigh-like response within a certain range of the E-field amplitudes and frequency (1 – 10^4 Hz). A typical response is displayed in Figure 2 (a), showing increasing dielectric permittivity with increasing E-field amplitude and decreasing frequency. The variation of the corresponding Rayleigh parameters ($\varepsilon_r'(0)$ and α) is shown for all samples at various stages of their post-treatments in Figure 2 (b) and (c), as correlated by equation (2). The results show the influence of texture, sample orientation with respect to the direction of applied electric field, and the state of poling on the linear (Figure 2 (a)) and nonlinear (Figure 2(b)) contributions to the small signal dielectric response. Generally, the non-textured sample showed the highest dielectric permittivity, though with very high nonlinear contribution. When the electric field is applied in different directions of the textured specimens (i.e., the PTC and VTC specimens), there is a significant difference in the reversible ($\varepsilon_r'(0)$) and irreversible (α) contributions to the longitudinal

dielectric permittivity. This difference is however reduced after high temperature poling. As a general tendency, the VTC sample yields higher linear contribution ($\varepsilon_r'(0)$) and lower non-linear contribution (α) to the dielectric response, respective to the PTC sample; this trend is especially pronounced in the non-poled state. The VTC and PTC samples are fabricated from the same larger samples and thus have identical composition and microstructure, hence the differences observed between the textured PTC and VTC samples originate from the intrinsic and extrinsic anisotropic properties, and not from microstructural or compositional differences. The processing of the non-textured sample was different from that of the PTC and VTC samples, which might result in slightly different microstructure and composition, and therefore, electrical properties. A direct comparison of the experimentally measured response between the textured and non-textured samples is therefore not straightforward.

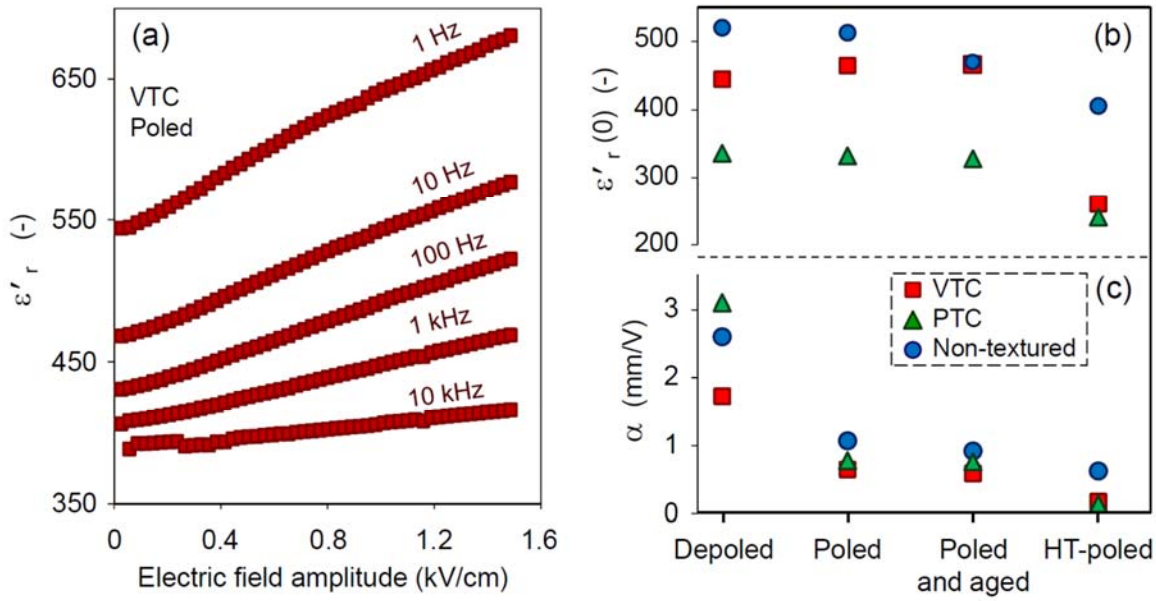

Figure 2. (a) Typical electric field amplitude dependence of the relative dielectric permittivity at the measured frequencies for KNN (a case of the VTC-textured KNN). (b) Initial permittivity and (c) Rayleigh constant at the different sample stages for textured (VTC and PTC) and non-textured KNN at 100 Hz and E_0 = kV/cm.

3.2 Intrinsic contributions

Differences in the dielectric and piezoelectric responses of the PTC and VTC samples can be rationalized considering the anisotropy of the corresponding tensorial property coefficients and the preferred orientation of crystallites within each configuration. The distributions of the polar vectors (P_s) in an ideally textured ceramic (perfectly oriented) are schematically illustrated in Figure 3 (a-b) for the three types of sample configurations addressed. The P_S distributions in the unpoled samples (Figure 3 (a)), generally categorized as type "disc," "cone," or "sphere," can be constructed by considering all possible orientations of crystallites in each sample configuration. The "cone" and "disc" type distributions in the textured specimens (PTC and VTC samples) are present because the needle-like templates used in the texture processing are randomly oriented in the angle about the tape casting axis. Figure 3 (b) shows the P_S distributions after poling and is constructed by assuming that only the polarization vectors most closely aligned to the electric field are retained after poling; polarization vectors in non-favorable directions are assumed in this representation to reorient into one of the more favorable directions.

While the distribution of P_S in the sample orientation space is instructive, it is also useful to illustrate the preferred orientation of P_S to E in the reference frame of the crystal. These directions are shown on a representative property surface in Figure 3 (c-d) using lines and areas on the properties surfaces of the calculated[20] longitudinal relative dielectric permittivity $(\varepsilon_r')^*_{33}$ and the longitudinal piezoelectric coefficient d^*_{33} for a prototype for $KNbO_3$ single crystal. The shown property surfaces were obtained by M. Budimir[20] using the Landau-Ginsburg-Devonshire theory[21,22] and the previously calculated values of the dielectric constant[23] and electrostrictive coefficients[24] for a $KNbO_3$ single crystal. The experimental values of the dielectric anisotropy in $KNbO_3$, in terms of the dielectric constants measured along the principal axes, range as $\varepsilon'_{r(x_1)} \approx 870..1200$, $\varepsilon'_{r(x_2)} \approx 140..160$, and $\varepsilon'_{r(x_3)} \approx 40..55$.[20,23,25-27] The surfaces shown in Figure 3 (c-d) illustrate the

intrinsic orientation dependence of the longitudinal dielectric and piezoelectric coefficients. Lines and areas are overlaid on the representational surfaces that correspond to the distributions of possible electric field directions relative to the P_S of crystals. The intrinsic properties of an ideally textured material may be predicted as an average of all possible values identified by these lines and areas.

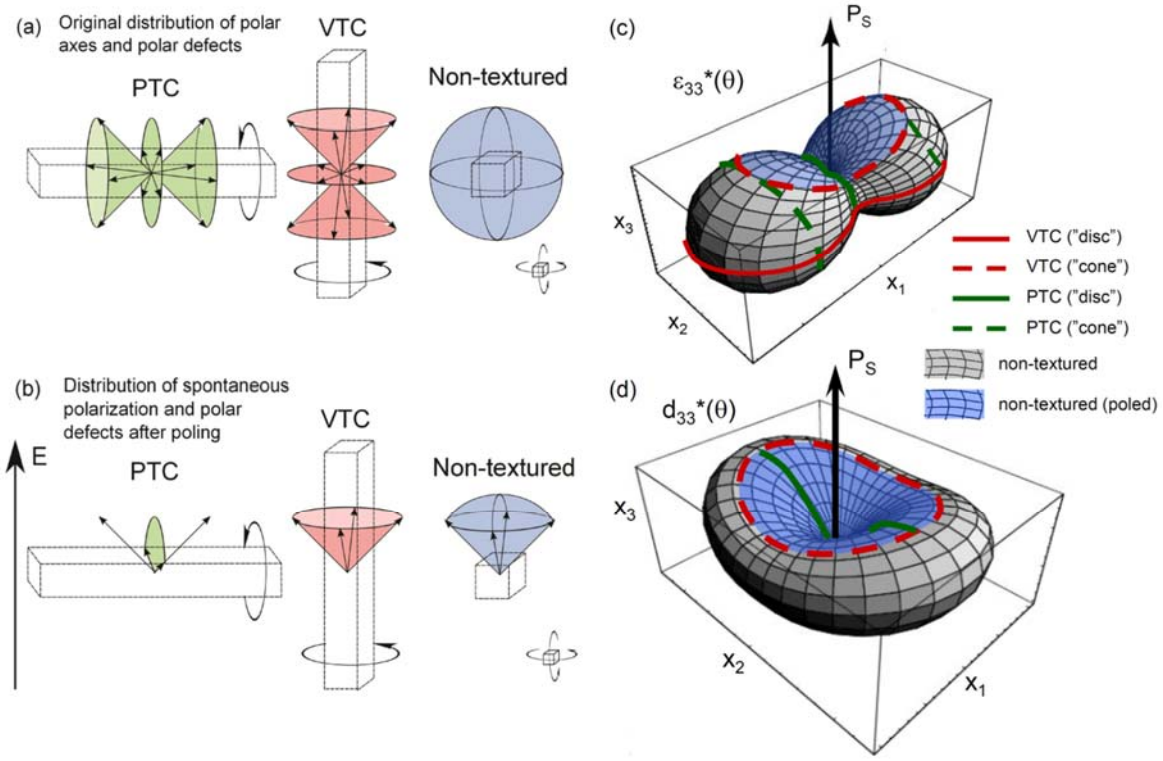

Figure 3. (a- b) Schematic of polar axes distributions in ideally textured and non-textured ceramics before (a) and after (b) poling. The cuboids represent the direction of elongated grains (created by templated grain growth onto needle-like templates) relative to the poling and electric field direction. (c-d) Calculated direction dependencies of $(\varepsilon_r')_{33}^*$ (c) and d_{33}^* (d) in the orthorhombic $KNbO_3$ prototype[20] (adapted with permission from M. Budimir Ph.D. dissertation, Swiss Federal Institute of Technology – EPFL, 2006. Copyright: reserved rights). Color contour lines indicate the directions of the electric field relative to the crystal coordinate reference frame in the PTC and VTC samples; the corresponding directions in the non-textured samples may cover either whole surface (in the unpoled state) or the blue surface segment (in the poled state).

We now use the representations in Figure 3 (c) to interpret some of the measured results for dielectric permittivity in Figure 2 (b). As illustrated in Figure 3 (c), the intrinsic dielectric response in the unpoled PTC sample is contributed from crystallites with P_S oriented in the "cones" and "discs" shown in Figure 3 (a). The contribution to intrinsic permittivity of crystallites with P_S oriented in the "cone" is larger than that from the crystallites with P_S oriented in the "disc." In contrast, in the unpoled VTC sample, a much larger contribution to the intrinsic permittivity is predicted from the crystallites with P_S oriented in the "disc": it contours a large perimeter on the $(\varepsilon_r')^*_{33}$ surface, contributing significantly to enhanced intrinsic dielectric response in VTC samples. By comparing the VTC and PTC representations in Figure 3 (c), a much higher intrinsic dielectric permittivity is expected in the VTC sample than in the PTC sample. This is indeed observed in Figure 2 (b), showing that the reversible contribution to dielectric permittivity (which includes the intrinsic component) in the VTC sample is consistently larger than that of the PTC sample. Thus, the higher intrinsic dielectric response measured in the VTC sample relative to the PTC sample originates from the collective contribution of P_S arrangements relative to the field direction in the textured specimen. Since non-textured and unpoled ceramics have a variety of crystal orientations parallel to the field direction (the outlined area in Figure 3 (c)), a hypothesis of their relative intrinsic dielectric permittivities is less straightforward.

A similar analysis can be undertaken to predict the intrinsic longitudinal piezoelectric coefficient when the electric field is applied in different directions of textured and poled specimens. Figure 3 (d) shows the representational property surface for the longitudinal piezoelectric coefficient and the orientation of the electric field relative to P_S for various sample configurations. Here, the intrinsic piezoelectric response in the VTC sample is expected to be considerably larger than that of the PTC sample confirmed by the measured piezoelectric coefficients in poled VTC and PTC samples (Table I). For the samples without initial grain texture, the overall intrinsic piezoelectric response in the poled specimens should originate from crystals with P_S randomly distributed in the area identified in Figure 3 (d). An average of these values might suggest that a similar or slightly

lower piezoelectric response may be expected relative to the poled PTC sample. However, the experimental values of the randomly oriented sample are higher than those of the PTC sample (Table 1). As mentioned above, a comparison between property measurements in the textured and non-textured specimens is not straightforward, as they may not be identical in composition and microstructure.

3.3 Extrinsic contributions

To a first approximation, poling is expected to reduce the extrinsic contributions to permittivity by reducing the domain wall density and thus the overall contribution of the motion of domain walls to property coefficients. In addition, poling introduces domain texture (preferred orientation of domain variants) and thus affects the intrinsic contributions as well. As illustrated in Figure 3 (b), poling tends to align crystal orientations such that their P_S is as closely parallel to the E-field direction as possible through domain reorientation. This reorientation during poling has consequences to the contributions of intrinsic effects and extrinsic domain walls during subsequent property measurements. For example, the poling of the VTC sample reduces the fraction of crystals with P_S oriented perpendicular to the field direction (within the "disc"), the orientations that contribute most to the intrinsic dielectric response (Figure 3 (c)). Removing these most dielectrically strong orientations should result in a lower intrinsic contribution to permittivity in poled VTC samples. Hence poling may be expected to reduce both the intrinsic and extrinsic contributions to the permittivity. Figure 2 (b-c) shows that with the increasing strength of the poling treatment decreases $\varepsilon_r'(0)$ and α, consistent with these expectations.

The domain configuration imposed by poling can also be stabilized by rearrangement of point defects interacting with the spontaneous polarization during aging.[28] Alternatively, the process may be accelerated at elevated temperatures, where mobility of both domain walls and point defects are enhanced. Domain stabilization and aging would lead to reduced extrinsic effects. Figure 2(c) does not show a dramatic reduction with aging, but is still consistent with such an interpretation. In

addition, the influence of spontaneous strain anisotropy is expected to be lower at elevated temperature and may reducing the tendency of mechanical constraints to hinder the degree of poling through mechanical clamping.[29]

The relatively small effect of room-temperature poling on $\varepsilon_r'(0)$ suggests either incomplete P_S alignment during the poling, and/or a sustained high level of contribution from reversible domain wall motion. However, after poling at high temperature, a significant decrease of both the reversible and irreversible contributions is observed. This result may suggest that high temperature is necessary to provide sufficient driving force for large-scale domain wall motion and to obtain a highly poled state. Furthermore, the domain configuration in this highly poled state is expected to be stabilized by electrostatic arrangement of point defects[30-32], and thus reduce both the reversible and irreversible domain wall motion at room temperature (Figure 2 (c)). This indication of higher domain wall mobility at elevated temperatures is consistent with the known sluggish domain wall motion in KNN at room temperature.[33]

3.4 Discussion

The VTC sample, which has the highest density of pseudo-cubic <100> poles parallel to the E-field, demonstrated the lowest dielectric nonlinearity among all the three samples at all poling states (Figure 2 (c)). This suggests that the orientation-dependence in crystallographically textured specimens, such as the VTC sample in the present work, may be used to exploit the advantages of both the enhanced intrinsic dielectric and piezoelectric responses (Figure 3 (c) and (d)), while concurrently reducing the dielectric nonlinearity. The optimum response in the VTC sample is likely due to the reduced number of domains available for switching towards the direction of applied E-field (lowering the extrinsic contributions) while hosting the most ideal preferred orientation to achieve the highest intrinsic response. Indeed, domain switching in the orthorhombic KNN ceramics implies the polarization to choose one of 12 possible $[011]_c$ axes, the most close to the direction of

E-field. Figure 3 (a) shows that VTC sample has 1/3 of the P_S distribution already aligned with respect to the E-field direction (the upper or lower "cones", depending on the field polarity). Thus, only the remaining 2/3 of the domains are able to switch and may contribute to the nonlinearity. For comparison, the P_S distribution in random oriented orthorhombic ceramics allows switching for the domains with P_S diverging more than ±45° from the E-field direction, which is ~85% of the total number. Texturing in the VTC sample therefore reduces the number of domains contributing to the nonlinearity of polarization response while optimizing the intrinsic response.

While the present work focuses on analyzing dielectric nonlinearity in textured KNN created through needle-like templates, the approach and analysis methods presented in the present work can be adopted for other texture types, sample configurations, compositions, and physical properties. For example, textured KNN synthesized with plate-like templates creates a fiber texture wherein all directions within the tape casting plane are identical.[34] The expected dielectric nonlinearities may be rationalized by considering the possible orientations of P_S relative to the sample coordinate reference frame (similar to Figure 3 (a-b)) and relative to the crystal coordinate reference frame (similar to Figure 3 (c-d)). Likewise, textured bismuth titanate ($Bi_4Ti_3O_{12}$) can be synthesized using plate-like templates which develops a fiber sample symmetry during sintering.[35] The P_S directions in bismuth titanate are within the plane of the template, meaning that the nonlinearities in the in-plane and out-of-plane directions may be significantly different. Such a hypothesis is consistent with previously reported results for domain wall motion during application of strong electric field amplitudes.[18] In all of these systems, however, other mechanisms may be found to dominate or constrain the response, e.g. possible anisotropic pinning of domain walls by grain boundaries. Nevertheless, the approach taken in the present work provides a framework through which to discuss such results.

4 Conclusion

In conclusion, textured $K_{0.5}Na_{0.5}NbO_3$ (KNN) with a high degree of $<100>_{pc}$ texture parallel to the E-field direction was shown to increase the intrinsic dielectric and piezoelectric response and reduce the nonlinearity. The reduced nonlinearity is caused by the preferred orientation of the polar axes due to the grain texture, which reduces the likelihood of further domain wall motion at subswitching conditions. These results were shown to correspond well with previously calculated anisotropy of the dielectric permittivity in $KNbO_3$. This study therefore provides a framework to evaluate the effect of texture on nonlinear behavior in piezoelectric ceramics. Furthermore, the effects of poling, depoling, and aging on the polarization response of KNN ceramics with various textures have also been investigated and discussed.

Acknowledgements

The authors thank Gerhard Olsen and Professor Tor Grande for useful discussion and comments to the manuscript. Financial support from the Norwegian Research Council, grant no. 197497/F20 "Lead-free piezo- and ferroelectric $K_{0.5}Na_{0.5}NbO_3$" is acknowledged.

References

1 G. H. Haertling, *J. Am. Ceram. Soc.* **82,** 797 (1999).
2 D. A. Hall, *J. Mater. Sci.* **36,** 4575 (2001).
3 D. C. Lupascu and M. I. Morozov, in *Ceramics Science and Technology* (Wiley-VCH Verlag GmbH & Co. KGaA, 2010), p. 729.
4 A. Pramanick, D. Damjanovic, J. E. Daniels, J. C. Nino, and J. L. Jones, *J. Am. Ceram. Soc.* **94,** 293 (2011).
5 D. Damjanovic, *J. Am. Ceram. Soc.* **88,** 2663 (2005).
6 E. I. Bondarenko, V. Y. Topolov, and A. V. Turik, *Ferroelectrics Lett.* **13,** 13 (1991).
7 T. J. Yang, V. Gopalan, P. J. Swart, and U. Mohideen, *Phys. Rev. Lett.* **82,** 4106 (1999).
8 H. Ma, W.-J. Kim, J. S. Horwitz, S. W. Kirchoefer, and J. Levy, *Phys. Rev. Lett.* **91,** 217601 (2003).
9 F. Preisach, *Z. Physik* **94,** 277 (1935).
10 L. Rayleigh, *Philos.Mag. Series* **23,** 225 (1887).
11 D. Damjanovic and M. Demartin, *J. Phys. D-Appl. Phys.* **29,** 2057 (1996).
12 D. Damjanovic, *J. Appl. Phys.* **82,** 1788 (1997).
13 D. A. Ochoa, J. E. Garcia, R. Perez, V. Gomis, A. Albareda, F. Rubio-Marcos, and J. F. Fernandez, *J. Phys. D-Appl. Phys.* **42,** 025402 (2009).
14 B. Peng, Z. Yue, and L. Li, *J. Appl. Phys.* **109,** 054107 (2011).
15 K. Keisuke, H. Keiichi, M. Youichi, and A. R. Clive, *Appl. Phys. Express* **5,** 031501 (2012).
16 G. L. Messing, S. Trolier-McKinstry, E. M. Sabolsky, C. Duran, S. Kwon, B. Brahmaroutu, P. Park, H. Yilmaz, P. W. Rehrig, K. B. Eitel, E. Suvaci, M. Seabaugh, and K. S. Oh, *Crit. Rev. Solid State Mat. Sci.* **29,** 45 (2004).

[17] D. M. Marincel, H. Zhang, A. Kumar, S. Jesse, S. V. Kalinin, W. M. Rainforth, I. M. Reaney, C. A. Randall, and S. Trolier-McKinstry, *Adv. Funct. Mater.* **24,** 1409 (2014).
[18] J. L. Jones, B. J. Iverson, and K. J. Bowman, *J. Am. Ceram. Soc.* **90,** 2297 (2007).
[19] A. B. Haugen, G. H. Olsen, F. M. Madaro, M. I. Morozov, G. Tutuncu, J. L. Jones, T. Grande, and M. A. Einarsrud, *J. Am. Ceram. Soc.***,** Available as Early View online. DOI: 10.1111/jace.13223.
[20] M. Budimir, Thesis, EPFL, 2006.
[21] A. F. Devonshire, *Philos. Mag.* **40,** 1040 (1949).
[22] A. F. Devonshire, *Philos. Mag.* **42,** 1065 (1951).
[23] T. Fukuda, H. Hirano, Y. Uematsu, and T. Ito, *Jpn. J. Appl. Phys.* **13,** 1021 (1974).
[24] P. Günter, *Jpn. J. Appl. Phys.* **16,** 1727 (1977).
[25] S. Wada, K. Muraoka, H. Kakemoto, T. Tsurumi, and H. Kumagai, *Jpn. J. Appl. Phys.* **43,** 6692 (2004).
[26] E. Wiesendanger, *Ferroelectrics* **6,** 263 (1973).
[27] M. Zgonik, R. Schlesser, I. Biaggio, E. Voit, J. Tscherry, and P. Gunter, *J. Appl. Phys.* **74,** 1287 (1993).
[28] L. Jin, F. Li, and S. Zhang, *J. Am. Ceram. Soc.* **97,** 1 (2014).
[29] G. Tutuncu, B. Li, K. Bowman, and J. L. Jones, *J. Appl. Phys.* **115** (2014).
[30] P. V. Lambeck and G. H. Jonker, *Ferroelectrics* **22,** 729 (1978).
[31] K. Carl and K. H. Hardtl, *Ferroelectrics* **17,** 473 (1977).
[32] U. Robels and G. Arlt, *J. Appl. Phys.* **73,** 3454 (1993).
[33] W. Jo, R. Dittmer, M. Acosta, J. Zang, C. Groh, E. Sapper, K. Wang, and J. Rödel, *J. Electroceram.* **29,** 71 (2012).
[34] Y. Chang, S. Poterala, Z. Yang, and G. L. Messing, *J. Am. Ceram. Soc.* **94,** 2494 (2011).
[35] S.-H. Hong, S. Trolier-McKinstry, and G. L. Messing, *J. Am. Ceram. Soc.* **83,** 113 (2000).